ACS APPLIED MATERIALS & INTERFACES

Research Article

www.acsami.org

Lead Lanthanum Zirconate Titanate Ceramic Thin Films for Energy Storage

Sheng Tong,*[,†] Beihai Ma,[‡] Manoj Narayanan,[‡] Shanshan Liu,[‡] Rachel Koritala,[§] Uthamalingam Balachandran,[‡] and Donglu Shi[†]

[†]College of Engineering and Applied Science, University of Cincinnati, Cincinnati, Ohio 45221, United States

[‡]Energy Systems Division and [§]Nanoscience and Technology Division, Argonne National Laboratory, Argonne, Illinois 60439, United States

ABSTRACT: An acetic-acid-based sol–gel method was used to deposit lead lanthanum zirconate titanate (PLZT, 8/52/48) thin films on either platinized silicon (Pt/Si) or nickel buffered by a lanthanum nickel oxide buffer layer (LNO/Ni). X-ray diffraction and scanning electron microscopy of the samples revealed that dense polycrystalline PLZT thin films formed without apparent defects or secondary phases. The dielectric breakdown strength was greater in PLZT thin films deposited on LNO/Ni compared with those on Pt/Si, leading to better energy storage. Finally, optimized dielectric properties were determined for a 3-μm-thick PLZT/LNO/Ni capacitor for energy storage purposes: DC dielectric breakdown strength of ~1.6 MV/cm (480 V), energy density of ~22 J/cc, energy storage efficiency of ~77%, and permittivity of ~1100. These values are very stable from room temperature to 150 °C, indicating that cost-effective, volumetrically efficient capacitors can be fabricated for high-power energy storage.

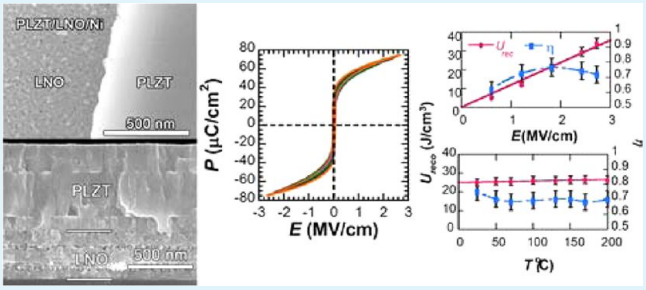

KEYWORDS: *PLZT, energy storage, thin film, capacitor, relaxor ferroelectric, base metal substrate*

Downloaded by UNIV OF CINCINNATI on August 31, 2015 | http://pubs.acs.org
Publication Date (Web): February 18, 2013 | doi: 10.1021/am302985u

INTRODUCTION

Because of climate change and global air pollution, intense effort is underway to replace high-CO_2-emission fossil fuel energy resources with cleaner renewable energy sources, such as solar and wind energy technology, as well as hybrid electric vehicles. For the purpose of stationary energy storage and vehicle propulsion, the demand for high efficient electric energy storage is on the rise. Broadly, there are two classes of energy storage: short term and long term.[1−3] The former is usually in the form of batteries, whereas the latter is usually in the form of capacitors, which are able to smooth out momentary fluctuations and ensure a stable supply of energy from renewable sources. Having orders of magnitude higher electric power density and cycle life compared with batteries, capacitors can be used to prolong the lifetime of batteries and improve the reliability of electric systems in hybrid vehicles, meet peak power needs in hybrid and electric vehicles, and keep internal combustion engines operating at an optimized energy efficiency. Although the battery-capacitor system has already been adopted widely in hybrid vehicles, more attention is now being directed toward improving overall performance while reducing module size, weight, and cost. Some of the desired improvements include increasing energy density, decreasing electrical and thermal losses, improving packaging, and improving reliability and lifetime.[3,4]

At present, polymer and electrolyte capacitors are often used for high-power output applications because of their high breakdown voltage and energy density. Advanced materials, e.g., supercapacitors, are considered a promising candidate to take the place of the battery-capacitor systems. However, to increase their reliability and energy efficiency, more advanced materials and techniques are required. Polymer capacitors usually exhibit low permittivity and low mechanical tolerance and must be operated within a limited temperature range. Electrolyte capacitors usually operate at low pulse repetition rate, suffer from voltage reversal, and have limited lifetime. Supercapacitors have low single-cell electric potential and packaging limitations.[1,5−7] By contrast, ceramic capacitors exhibit superior mechanical and thermal properties and orders-of-magnitude higher permittivity, and are thus considered the potential best candidate for the high-power energy storage application.[8] Yet, in the form of bulk and thick films (e.g., traditional multilayer ceramic capacitors), mainly $BaTiO_3$ ceramics, they are not able to withstand high electric fields, leading to a relatively low energy density.[9,10] Fortunately, the improvement of the circuit design for hybrid vehicles has resulted in lower operation voltage, down to subkilovolt levels, and durations, up to milliseconds. It is now possible to produce thin-film ferroelectric capacitors demonstrating many attractive properties, such as high capacitance, low remanent voltage, high breakdown strength, and low package volume. To better

Received: December 5, 2012
Accepted: February 4, 2013
Published: February 4, 2013

 © 2013 American Chemical Society

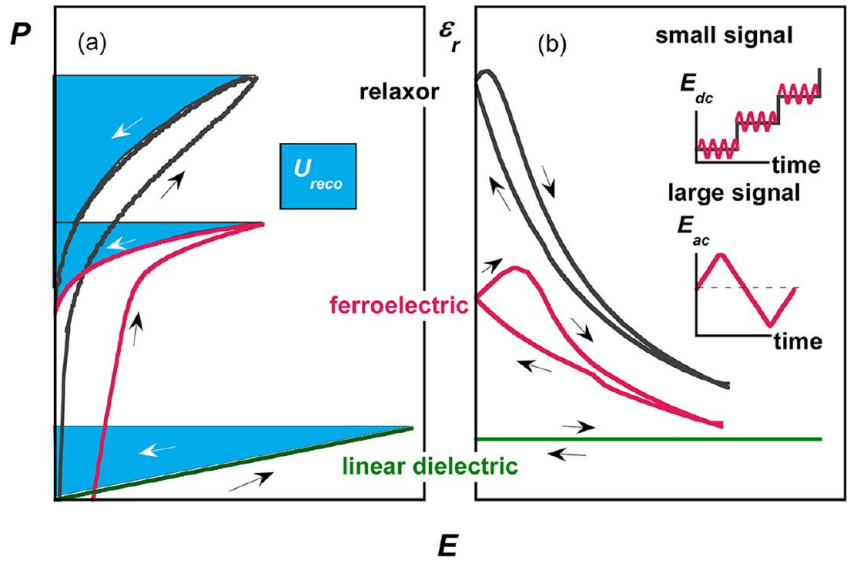

Figure 1. Typical dependence of (a) polarization and (b) permittivity on electric field for linear dielectric, ferroelectric, and relaxor. Inset in (b) is the small signal for capacitance−voltage ($C-V$) loop and large signal for the polarization-electric field ($P-E$) loop electric field as a function of time.

Downloaded by UNIV OF CINCINNATI on August 31, 2015 | http://pubs.acs.org
Publication Date (Web): February 18, 2013 | doi: 10.1021/am302985u

understand the advantages of the ferroelectric thin film capacitors, we explained the energy storage mechanism below.

Figure 1 shows the typical polarization and permittivity versus electric field for three compositions: linear dielectric with constant permittivity (e.g., Al_2O_3, glass, polymers), ferroelectric with spontaneous polarization (e.g., $BaTiO_3$), and relaxor with nanosized domains [e.g., $(Pb,La)(Zr,Ti)O_3$] materials. The electric energy stored per unit volume of a capacitor, U, is given by

$$U = \int_{P_1}^{P_2} EdP \tag{1}$$

where E is the electric field, and P is the polarization. When the electric field increases from zero to the maximum E_{max}, the polarization increases to the maximum P_{max}, and electric energy is stored in the capacitor as U_{store}. The recoverable electric energy density U_{reco} is then released on discharge from E_{max} to zero, represented by the shaded area in Figure 1a.

One can define the energy storage efficiency η as

$$\eta = \frac{U_{reco}}{U_{store}} \times 100\% \tag{2}$$

Also, since the permittivity (ε_0 and ε_r) is defined as dP/dE,

$$U = \int_{E_1}^{E_2} \varepsilon_0 \varepsilon_r EdE \tag{3}$$

Although eqs 1 and 3 are interchangeable in theory, in practice, polarization and permittivity are tested in large and small signal modes (see insets in Figure 1b). The former usually refers to a dynamic AC response, whereas the latter corresponds to a static DC bias voltage. The permittivity calculated for the large signal mode can be more than 100 times larger than that for the small signal mode.[11]

As seen in Figure 1a, b, linear dielectrics are considered one of the most effective dielectrics for energy storage because of the high breakdown strength, low dielectric and energy loss. However, in practice, the linear dielectrics usually have low permittivity and energy density[12] or wide hysteresis loops with low energy efficiency.[13,14] Ferroelectrics exhibit high permittivity but also high coercive electric field (E_c) and remanent polarization (P_r)[15] contributing to large energy loss. In contrast, relaxors exhibit high permittivity and slim hysteresis loops.[16,17] For thin-film relaxors in the energy storage application, their large permittivity can be taken advantage of by improving the breakdown strength.

Lead lanthanum zirconate titanate (PLZT) is considered to be one of the most significant A-site-substituted lead zirconate titanate (PZT) relaxors.[16] The doping of lanthanum decreases the lead usage, enhances the electrical reliability, and improves the temperature-dependent dielectric and ferroelectric properties. For years, the high permittivity and spontaneous polarization of these materials have attracted interest in their application as capacitors. Several reports on PLZT based relaxor ferroelectrics have been reported for energy storage applications.[18−21] Hao et al.[19] reported high energy storage capability of ∼30 J/cm^3 and efficiency of ∼60% in PLZT (9/65/35) thin films deposited on Pt/Si; Yao et al.[20] investigated both the energy and power capabilities of the antiferroelectric PLZT (2/95/5) thin films; Kim et al.[21] studied PLZT (7/62/38) on LNO buffered nickel substrates and achieved high capacitance density of ∼2.4 μF/cm^2. These authors reported the possibility of using ceramic thin film capacitors for high energy storage application. However, to our knowledge, key energy storage parameters of relaxor ferroelectric thin film capacitors, namely energy density and efficiencies, leakage current density, in a wide range of temperature have not been investigated or reported. The present work mainly focuses on the dielectric and ferroelectric properties of PLZT 8/52/48 ($Pb_{0.92}La_{0.08}Zr_{0.52}Ti_{0.48}O_3$) relaxor films deposited on substrates composed of platinized silicon (Pt/Si) and lanthanum nickel oxide buffered nickel (LNO/Ni) in a range of thicknesses. The LNO-buffered layer, a conductive metal oxide, inhibits diffusion between the nickel substrate and PLZT film, making air-atmosphere sintering possible.[22,23] On the basis of our results, optimum PLZT film capacitors can be determined with the proper combination of substrate/electrode/dielectric that will achieve the desired dielectric and ferroelectric properties required for fabrication of cost-effective volumetrically efficient capacitors with high charge density and high energy density.

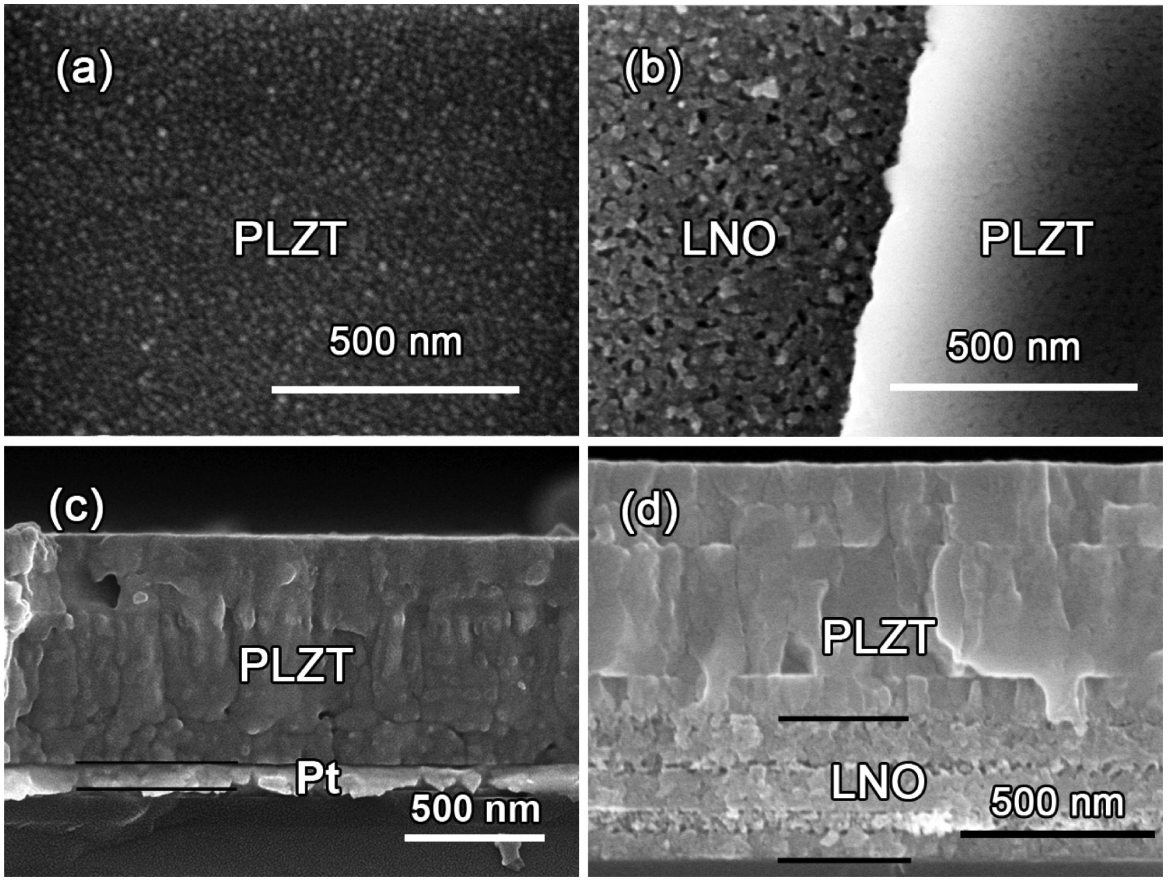

Figure 2. Planar SEM images of PLZT thin films coated on (a) Pt/Si and (b) LNO/Ni; cross-sectional SEM images of PLZT thin films deposited on (c) Pt/Si and (d) LNO/Si.

EXPERIMENTAL SECTION

$Pb_{0.92}La_{0.08}(Zr_{0.52}Ti_{0.48})O_3$ thin films with different thicknesses were deposited on Pt/Si and LNO/Ni. The Pt/Si substrates were cut from 10 cm dia wafers with ∼0.4 mm thickness (Nova Electronic Materials, Flower Mound, TX). The wafer consists of ∼100 nm thick Pt and ∼20 nm thick TiO_2 on silicon. Nickel substrates (99.8% pure) were polished to 1 μm finish (∼0.4 mm final thickness). Acetic acid wet chemistry was employed to prepare the LNO and PLZT precursor solutions.

A 0.3 M $LaNiO_3$ precursor solution was prepared by dissolving an appropriate molar ratio of lanthanum nitrate hexahydrate and nickel acetate tetrahydrate into acetic acid at 105 °C and stirring the mixture for 90 min. The LNO precursor solution was dispersed by syringe through a 0.02-μm pore size Anotop filter and spun coated onto a nickel substrate at 3000 rpm for 30 s. Each coating was pyrolyzed at 325 °C for 10 min and crystallized at 625 °C for 5 min. This process was repeated three times to build a buffer layer with thickness of ∼0.4 μm after final crystallization at 625 °C for 20 min.

A 0.5 M PLZT (8/52/48) solution was prepared with 20 mol % excess lead to compensate for the lead loss during crystallization heat treatments. In brief, zirconium n-propoxide and titanium isopropoxide were first mixed and chelated with acetic acid. Lead acetate and lanthanum acetate were mixed in sequence in acetic acid and dissolved by heating to 105 °C. Appropriate amounts of 1-propanol and deionized water yielded a 7:7:1 volume ratio of acetic acid, 1-propanol, and water to achieve a final concentration of 0.5M. PLZT layers were prepared by spin-coating the stock solution through a 0.02 μm filter onto platinum-coated silicon (PtSi) at 3000 rpm for 30 s. Each layer was pyrolyzed at 325 °C for 10 min and crystallized at 625 °C for 5 min. The films were crystallized for an extra 5 min every three layers. This process was repeated to achieve films of desired thickness, and the films were exposed to a final crystallization anneal of 625 °C for 15 min to ensure uniform perovskite phase. Platinum top electrodes (250-μm diameter and 100 nm thickness) were deposited through a shadow mask by e-beam evaporation.

Dielectric and other performance properties were measured with an Agilent N5751A DC Power Supply and Agilent E4980A LCR meter using an oscillator level (V_{ac}) of 0.1 V, a Radiant Precision Premier II system at 1 kHz, and a Keithley 237 high-voltage source meter, in conjunction with a Signatone QuieTemp probe station with hot stage. Phase identification was carried out using a Bruker AXS X-ray diffractometer (XRD) with General Area Detector Diffraction System, whereas microstructure and thickness were determined with a Hitachi S4700 field-emission scanning electron microscope (SEM).

RESULTS AND DISCUSSION

Planar and cross-sectional SEM images of representative PLZT films deposited on both substrates are given in Figure 2. The surface morphology of the films was smooth. Dense and uniform grains were visible without any obvious secondary phase. The average surface grain sizes of the PLZT thin films deposited on the Si and Ni substrates were measured to be ∼35 and ∼30 nm, respectively. The cross-sectional SEM images of PLZT shown as in Figure 2c and d exhibit dense and columnar grains due to the heterogeneous nucleation growth. Micrometer-sized secondary phases like pyrochlore/fluorite phases[26] were not observed in the SEM images. These observations were also confirmed by the lack of corresponding diffraction peaks in XRD scans and the demonstration of excellent dielectric properties, as discussed below. The surface SEM image of the LNO thin film in Figure 2b is partially dense with nanosized pores. The LNO grain size is ∼32 nm. Figure 2d reveals that

Downloaded by UNIV OF CINCINNATI on August 31, 2015 | http://pubs.acs.org
Publication Date (Web): February 18, 2013 | doi: 10.1021/am302985u

the LNO thin film is dense throughout the layered cross section with fine spherical grains. This microstructure is seen in many other solution-derived LNO thin films and proved to do no harm to the conductivity of these metal oxide thin films.[24,25] Similar microstructures of wet-chemical-derived heterostructures of PZT/Pt/Si and PZT/LNO/Si have also been reported.[27,28]

The indexed XRD patterns in Figure 3 indicate the formation of phase-pure perovskite with a pseudocubic structure in LNO

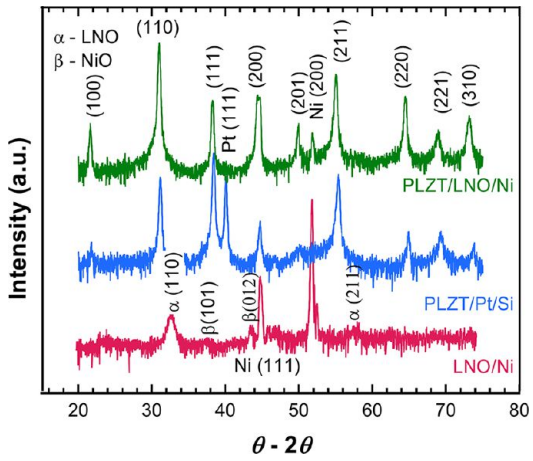

Figure 3. XRD patterns of ~3 μm PLZT thin films coated on LNO/Ni and Pt/Si, and ~0.4 μm LNO thin films coated on nickel.

thin films on nickel and PLZT thin films fabricated on both substrates. The XRD patterns indicated that the LNO and PLZT thin films are polycrystalline and randomly oriented. These observations are confirmed by the SEM images (Figure 2). The peaks of LNO thin films are wide with low intensity, consistent with the nanosized grains seen in the SEM images, whereas the peaks of PLZT thin films are sharp and high, accounting for the extremely dense columnar grains in the PLZT thin films.

The XRD patterns and SEM images confirm the phase purity, uniformity, and denseness of LNO and PLZT thin films. These properties are important in the permittivity, dielectric breakdown strength, permittivity, and energy loss of the ceramic thin film capacitors, which are the main performance parameters used in assessing capacitive energy storage.

The capacitance–voltage (C–V) loops of PLZT thin films on the different substrates are illustrated in Figure 4, featuring well-defined butterfly loops that saturate at high electric field with good dielectric tunability. As the inset in Figure 1b shows, the C–V testing involves applying an AC small signal (V_{ac} = 0.1 V) and the step-increased DC voltage (V_{dc}). Thus, the permittivity, dielectric loss, and corresponding electric energy density under the small signal testing are considered to be static values, in contrast to the large signal used in polarization-electric field (P–E) hysteresis loop testing. When E_{dc} is increased from 0 to 0.4 MV/cm at room temperature, as seen in Figure 4a, the permittivity (capacitance density) values of PLZT/Pt/Si thin films decrease from ~1400 to 500 (~1.2 to 0.44 F/cc), whereas those for PLZT/LNO/Ni decline from ~1000 to 500 (~0.88 to 0.44 F/cc). At E_{dc} = 0 and 0.4 MV/cm and room temperature, the dielectric loss values are 0.07 and 0.03 for PLZT/LNO/Ni and 0.05 and 0.03 for PLZT/Pt/Si, respectively. As shown in Figure 4b, when the temperature increases to 150 °C at E_{dc} = 0, the permittivity (capacitance

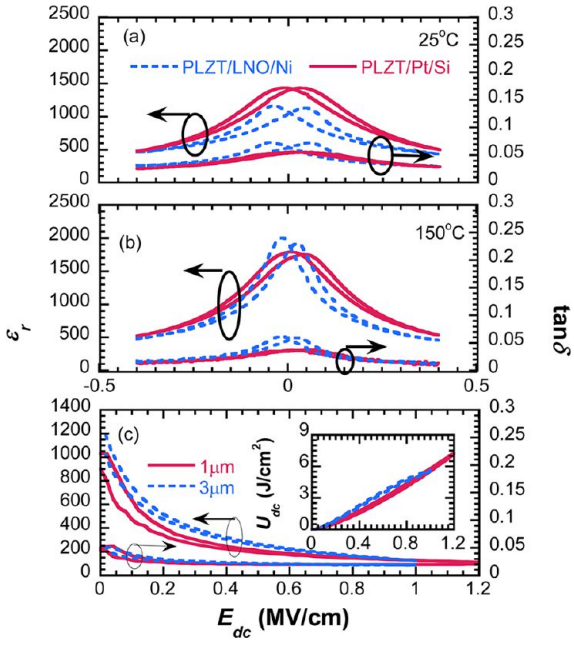

Figure 4. C–V loops of ~1-μm-thick PLZT thin films coated on (a) Pt/Si and (b) LNO/Ni; (c) high electric field C–V loops of PLZT/LNO/Ni. Inset in (c) is the calculated U_{dc} corresponding to the plotted permittivity values. All measurements carried out at 10 kHz.

density) of PLZT thin films deposited on Pt/Si and LNO/Ni increases to ~1700 and 1800 (~1.5 and 1.6 F/cc), and the dielectric loss decreases to 0.3 and 0.5, respectively. The values at 150 °C are close to those at room temperature and E_{dc} = 0.4 MV/cm, indicating that the dielectric properties are less dependent on temperature under a DC bias electric field. As shown in Figure 4c, we also tested the PLZT/LNO/Ni with film thickness of 3 μm and DC electric field up to 1 MV/cm (300 V), as well as film thickness of 1 μm and DC electric field up to 1.2 MV/cm (120 V). The results indicate that our thin films display excellent quality for high field applications. The inset in Figure 4c illustrates the electric energy density calculated from eq 3 for E_{dc} from 0 to E_{max}. These energy densities reach as high as 5.6 and 7.3 J/cc in 3 and 1 μm thick PLZT/LNO/Ni thin films, respectively.

Figure 5 shows the dielectric properties of PLZT thin films on both substrates over a wide temperature range and E_{dc} range of 0–0.2 MV/cm. A maximum in permittivity values for PLZT/Pt/Si appears at ~150 °C. The permittivity of the PLZT/LNO/Ni has no maximum but increases with temperature. As the DC bias voltage increases, the permittivity and dielectric loss values decrease, and the permittivity vs temperature curves become flatter. At E_{dc} = 0.2 MV/cm over the temperature range, the permittivity values for PLZT/Pt/Si and PLZT/LNO/Ni decrease to ~900 and 500, whereas their dielectric loss tangents decrease to 0.02 and 0.03, respectively; these observations suggest that the permittivity and dielectric loss are almost temperature-independent.

Figure 6a shows the results from Weibull statistical failure analysis of dielectric breakdown of PLZT thin films coated on both substrates. As shown by Figure 6c, the breakdown strength was measured after voltage cycling (alternating every second between 0 and 2x V/s, where x = 1,2,3, ...), and then recording the field at which one observes an abrupt rise in leakage current (<1 mA) through the dielectric. The average DC breakdown fields (E_b), shown in Figure 6a, b, were

Downloaded by UNIV OF CINCINNATI on August 31, 2015 | http://pubs.acs.org
Publication Date (Web): February 18, 2013 | doi: 10.1021/am302985u

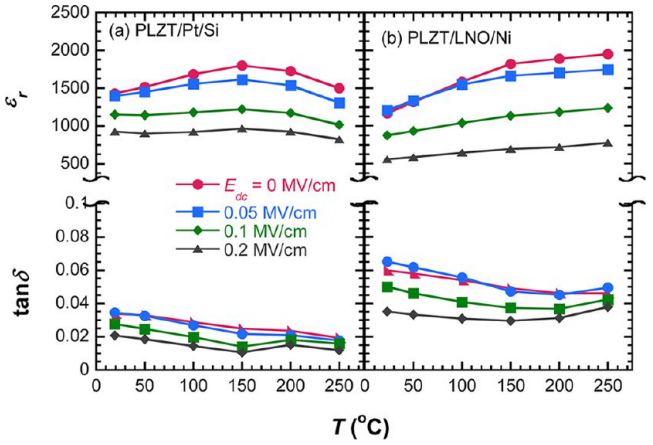

Figure 5. Dielectric properties of PLZT thin films coated on (a) Pt/Si and (b) LNO/Ni at 10 kHz as a function of temperature and E_{dc}.

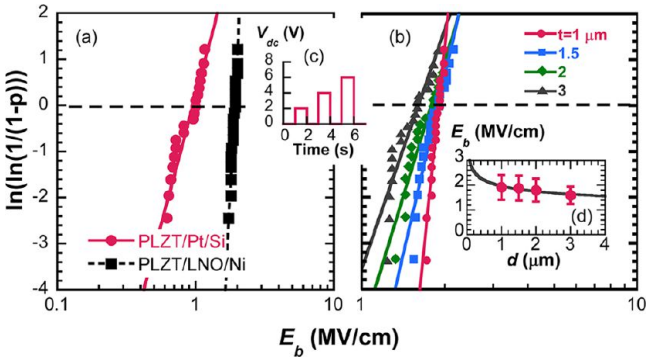

Figure 6. Weibull plots of dielectric breakdown of (a) ~1-μm-thick PLZT thin films coated on Pt/Si and LNO/Ni and (b) PLZT/LNO/Ni thin films of various thicknesses. Inset (c) shows voltage vs time used in the dielectric breakdown testing. Inset (d) shows the DC bias voltage as a function of thickness.

determined from fitting the experimental data to the empirical two-parameter Weibull cumulative distribution function for failure probability distribution[29]

$$p = 1 - \exp[-(E_b/\eta)^{\beta}] \quad (4)$$

$$p = (i - 0.3)/(n + 0.4) \quad (5)$$

where p is the sample cumulative distributive parameter, η and β are the fitting parameters, i is the sample sequence number, and n is the total sample number. The average E_b is determined at the value when $\ln(1/(1-p)) = 1$. The data indicate that the dielectric breakdown strength of PLZT/LNO/Ni (~1.96 MV/cm) is almost twice that for PLZT/Pt/Si (~1.00 MV/cm), indicating that PLZT/LNO/Ni is more favorable for energy storage applications. The dielectric breakdown strength observed is higher than that reported for many other PLZT thin film compositions.[19,20]

Figure 6b illustrates the effect of thickness on the breakdown strength of the PLZT/LNO/Ni. The data reveal that E_b decreases as the thickness increases, consistent with thermal breakdown theory. Scott et al.,[30] Yoshimura and Bowen,[31] and O'Dwyer[32] concluded that there is a power relationship between E_b and thickness, d

$$E_b = cd^{-\alpha} \quad (6)$$

where α and c are constants. Using the curve in Figure 6d, we calculated the fitting parameters as $\alpha \approx 0.166$ and $c \approx 1.962$ MV/cm. If the thickness is increased to bulk scale as 2 mm, the calculated E_b from eq 6 is ~0.5 MV/cm, which is close to the bulk breakdown strength of similar PZT ceramics.[30]

Figure 7 shows the hysteresis loops for high electric field ($E_{max} = E_b$) with different thickness of PLZT films coated on

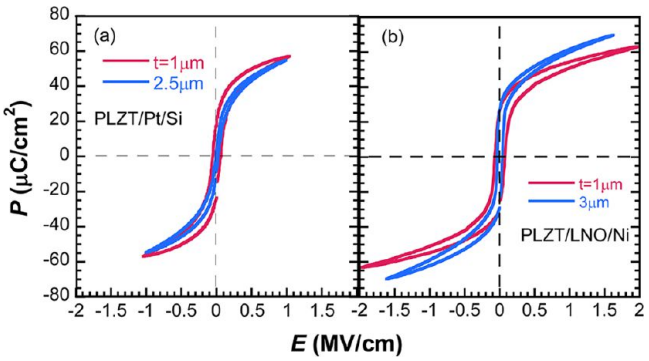

Figure 7. Hysteresis loops at high electric field (at $E_{max} = E_b$) for PLZT thin films coated on (a) Pt/Si and (b) LNO/Ni at 1 kHz and different film thickness.

Pt/Si and LNO/Ni . It is widely known that relaxors exhibit slim hysteresis loops, corresponding to small energy loss, and high permittivity, corresponding to high recoverable electric energy. As shown in Figure 7 and Table 1, the higher breakdown field produces a larger recoverable energy density in PLZT/LNO/Ni compared with PLZT/Pt/Si. Also, the thicker films formed slimmer hysteresis loops, leading to better energy efficiency, as shown in Table 1. It is interesting to find that although larger energies can be stored in thinner films, the discharged energies are greater for thicker films. Although the dielectric breakdown field decreases as film thickness increases, 3 μm thick PLZT/LNO/Ni is still favored for energy storage applications because of its higher breakdown voltage of ~480 V, high energy density of ~22 J/cc, and electric efficiency of ~77%. These values are higher than that reported in the literatures. For example, Hao et al.[19] reported similar energy density ~20 J/cc for PLZT (9/65/35) thin films, however the energy efficiency was <60% and Wang et al.[33] found that the antiferroelectric PLZT (2/98/2) exhibited higher energy density of ~25 J/cc, and much lower energy efficiency (~50%). Sigman et al.[34] also reported different compositions of PZT-based thin film capacitors, e.g. PZT (53/47), PLZT (12/70/30), with energy density of ~12.5 and 22 J/cc, respectively. Note that during the P–E hysteresis loop tests, we employed triangular signals, which are usually associated with higher breakdown strength than DC dielectric breakdown strength. Thus, a higher energy density is expected in the AC signal testing compared with DC signal measurement.

Table 1. Capacitive Energy Storage for PLZT Thin Films Deposited on Pt/Si and LNO/Ni Tested at $E_{max} = E_b$

	d (μm)	U_{reco}(J/cc)	η (%)
PLZT/LNO/Ni	3	22.0	77
	1	21.5	63
PLZT/Pt/Si	2.5	12.6	81
	1	9.8	55

Downloaded by UNIV OF CINCINNATI on August 31, 2015 | http://pubs.acs.org
Publication Date (Web): February 18, 2013 | doi: 10.1021/am302985u

Figure 8 plots permittivity and dielectric loss tangent as a function of frequency for 3 μm thick PLZT/LNO/Ni under

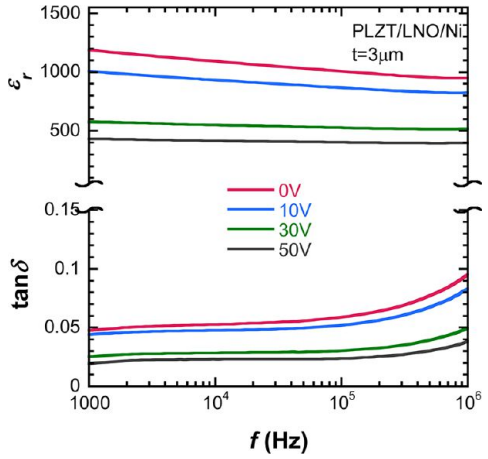

Figure 8. Frequency sweeps of PLZT/LNO/Ni under different DC bias voltages (V_{ac} = 0.1 V, f = 10 kHz).

DC bias voltages of 0−50 V. The curves for permittivity and dielectric loss are very stable in the testing range from 1 kHz to 1 MHz. As the DC bias voltage increases, the permittivity decreases from ∼1100 at 0 V to ∼400 at 50 V. Still, a permittivity of ∼400 is much higher than most of the dielectrics used for high electric field capacitors. Similarly, the dielectric loss decreases from ∼0.05 to ∼0.01, which is acceptable for short-time energy storage.

Because the pulse energy density is higher than that under $E_{max} = E_b$ since the AC breakdown strength is greater, we tested our 3-μm-thick sample at various E_{max} values, as shown in Figure 9a; the corresponding energy density and efficiency are

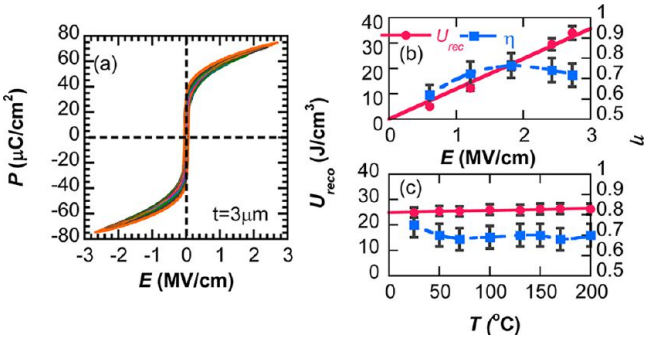

Figure 9. (a) Hysteresis loops of PLZ/LNO/Ni thin films under various E_{max}; (b) linear fitting of U_{reco} (red) and η (blue) as function of E_{max}; (c) linear fitting of U_{reco} (red) and η (blue) as function of temperature at E_{max} = 2 MV/cm.

shown in Figure 9b. The U_{reco} fit to the applied maximum electric field is linear (Figure 9b), where U_{reco} (J/cc) = 11.9 E_{max} (MV/cm). The efficiency reaches a maximum of ∼0.77 at E_{max} ∼2 MV/cm, at which U_{reco} ∼22 J/cc. It decreases further due to higher dielectric leakage. Fixing at E_{max} = 2 MV/cm, we tested U_{reco} and η as a function of temperature, with results shown in Figure 9c. The data reveal that the energy density and efficiency are almost independent of temperature and fixed at ∼25 J/cc and 0.7, respectively, similar to the permittivity and dielectric loss being temperature independent at a given DC bias voltage. These superior temperature dependent energy storage properties have not been reported previously. Hao et al.[19] reported that the energy density decreases from ∼11.5 to 9.5 J/cc when the temperature increased from 25 to 130 °C in the PLZT (9/65/35) thin films. Wang et al.[33] also observed a decreasing trend in the energy density (∼22 to 18 J/cc) of antiferroelectric PLZT (2/98/2) films with increase in temperature from 20 to 120 °C. In addition, the energy efficiencies reported were less than ∼60%. Hao et al.[35] also reported stable temperature dependent energy storage densities in antiferroelectric PLZT (2/95/5) with a relatively low energy density of ∼10 J/cc. These results provide strong support to our contention that our PLZT thin films are a promising candidate for capacitive energy storage over a wide temperature range.

When capacitors are used for high-electric-field energy storage, the dielectric leakage current density is an important parameter in determining the efficiency. We have plotted the DC leakage current density j as a function of time for E_{dc} = 0.1− 0.5MV/cm at room temperature (Figure 10a) and for T =

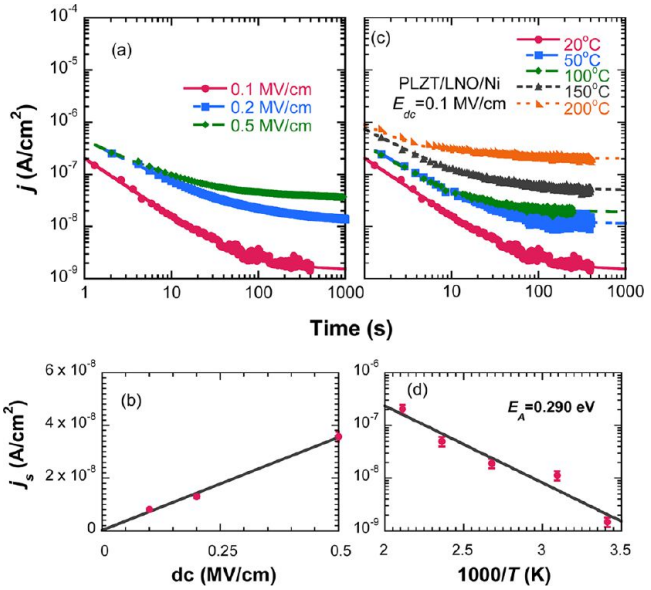

Figure 10. Dielectric relaxation of DC leakage current density of PLZT/LNO/Ni thin films under different (a) DC voltage bias and (c) temperature. Steady-state leakage current density vs (b) DC electric field and (d) temperature.

20−200 °C at E_{dc} = 0.1 MV/cm (Figure 10c). The leakage current density shows a strong initial time dependence because of dielectric polarization relaxation, which obeys the Curie-von Schweidler law as follows[36]

$$j = j_s + j_0 t^{-n} \quad (7)$$

where j_s is the steady-state current density, j_0 is a fitting constant, t is the relaxation time in seconds, and n is the slope of the log−log plot.

By fitting the leakage current density data at different DC bias voltages into eq 7, we found that the steady-state leakage current densities are linear with DC bias voltage (Figure 10b), mimicking Ohmic behavior. The observed leakage current densities of ∼3.5 × 10^{-8} A/cm^2 at 0.5 MV/cm is more than an order lower than that reported for PLZT thin films.[19] The data for the temperature-dependent leakage current density were fit into the Arrhenius equation

Downloaded by UNIV OF CINCINNATI on August 31, 2015 | http://pubs.acs.org
Publication Date (Web): February 18, 2013 | doi: 10.1021/am302985u

$$j_s = C\exp\left(-\frac{E_a}{kT}\right) \quad (8)$$

where C is a constant, E_a is the activation energy, k is the Boltzmann constant. The result yielded an activation energy of ~0.29 eV, which is close to previous values reported on PZT thin films.[37,38] The low leakage current density over a wide range of DC voltages and temperature further support the use of our thin-film capacitors. The high energy density/efficiency and low leakage current density in a wide temperature range indicates that the PLZT (8/52/48) thin films deposited on LNO buffered Ni substrates are a great candidate for high-power energy storage applications.

CONCLUSIONS

We fabricated PLZT thin film capacitors using acetic acid assisted sol–gel deposition on Pt/Si and LNO/Ni substrates. The test results indicated that our 3 μm thick PLZT/LNO/Ni capacitors possess the following attractive properties for capacitive energy storage: high dielectric breakdown electric voltage (~480 V) and field (~1.6 MV/cm), low dielectric loss (~0.05) and leakage current density (~1×10^{-8} A/cm^2), and high recoverable electric energy (~22 J/cc) and efficiency (~77%) on discharge. These properties indicate that our capacitors have strong potential application in hybrid/electric vehicles and power supplies.

AUTHOR INFORMATION

Corresponding Author

*E-mail: shengtg@mail.uc.edu. Phone: +1(630)252-4628.

Notes

The authors declare no competing financial interest.

ACKNOWLEDGMENTS

This work was supported by the U.S. Department of Energy, Vehicle Technologies Program, under Contract DE-AC02-06CH11357. The electron microscopy was accomplished at the Electron Microscopy Center for Materials Research at Argonne National Laboratory, a U.S. Department of Energy Office of Science Laboratory operated under Contract DE-AC02-06CH11357 by UChicago Argonne, LLC

REFERENCES

(1) Sarjeant, W.; Clelland, I. W.; Price, R. A. *Proc. IEEE* **2001**, *89*, 846–855.
(2) Ribeiro, P. F.; Johnson, B. K.; Crow, M. L.; Arsoy, A.; Liu, Y. *Proc. IEEE* **2001**, *12*, 1744–1756.
(3) Simon, P.; Gogotsi, Y. *Nat. Mater.* **2008**, *11*, 845–854.
(4) Jeffrey, W.; Dunn, B.; Rolison, D. R.; White, H. S. *Chem. Rev.* **2004**, *10*, 4463–4492.
(5) Kötz, R.; Carlen, M. *Electrochim. Acta* **2000**, *15*, 2483–2498.
(6) Zhang, Z.; Chung, T. C. M. *Macromolecules* **2007**, *40*, 783–785.
(7) Rabuffi, M.; Picci, G. *IEEE Trans. Plasm. Sci.* **2002**, *5*, 1939–1942.
(8) Love, G. R. *J. Am. Ceram. Soc.* **1990**, *2*, 323–328.
(9) Gao, F.; Dong, X.; Mao, C.; Liu, W.; Zhang, H.; Yang, L.; Cao, F.; Wang, G. *J. Am. Ceram. Soc.* **2011**, *12*, 4382–4386.
(10) Ogihara, H.; Randall, C. A.; Trolier-McKinstry, S. *J. Am. Ceram. Soc.* **2009**, *8*, 1719–1724.
(11) Schaab, S.; Granzow, T. *Appl. Phys. Lett.* **2010**, *97*, 132902.
(12) Chen, Q.; Wang, Y.; Zhou, X.; Zhang, Q. M.; Zhang, S. *Appl. Phys. Lett.* **2008**, *92*, 142909.
(13) Guan, F.; Pan, J.; Wang, J.; Wang, Q.; Zhu, L. *Macromolecules* **2010**, *43*, 384–392.
(14) Chu, B.; Zhou, X.; Ren, K.; Neese, B.; Lin, M.; Wang, Q.; Bauer, F.; Zhang, Q. *Science* **2006**, *5785*, 334–336.
(15) Auciello, O.; Scott, J. F.; Ramesh, R. *Phys. Today* **1998**, *51*, 22–27.
(16) Cross, L. E. Relaxor Ferroelectrics. In *Piezoelectricity*; Heywang, W., Lubitz, K.; Wersing, W., Ed.; Springer: Berlin, 2008; Vol. *114*, pp 131–155.
(17) Cohen, R. E. *Nature* **2006**, *22*, 941–942.
(18) Brennecka, G. L.; Ihlefeld, J. F.; Maria, J. P.; Tuttle, B. A.; Clem, P. G. *J. Am. Ceram. Soc.* **2010**, *93*, 3935–3954.
(19) Hao, X.; Wang, Y.; Yang, J.; An, S.; Xu, J. *J. Appl. Phys.* **2012**, *112*, 114111.
(20) Yao, K.; Chen, S.; Rahimabady, M.; Mirshekarloo, M. S.; Yu, S.; Tay, F. E. H.; Sritharan, T.; Lu, L. *IEEE Trans. Ultrason. Ferro. Freq. Contr.* **2011**, *58*, 1968–1974.
(21) Kim, S.-H.; Koo, C. Y.; Cheon, J. –H.; Ha, J.; Lee, J. –W.; Lee, I. –H.; Kim, W. S.; Wardle, B. L. *J. Korean Phys. Soc.* **2009**, *54*, 840–843.
(22) Ma, B.; Narayanan, M.; Balachandran, U. *Mater. Lett.* **2009**, *15*, 1353–1356.
(23) Narayanan, M.; Ma, B.; Balachandran, U.; Li, W. *J. Appl. Phys.* **2010**, *2*, 024103.
(24) Meng, X. J.; Sun, J. L.; Yu, J.; Ye, H. J.; Guo, S. L.; Chu, J. H. *Appl. Surf. Sci.* **2001**, *1*, 68–70.
(25) Miyake, S.; Fujihara, S.; Kimura, T. *J. Eur. Ceram. Soc.* **2001**, *10*, 1525–1528.
(26) Lefevre, M. J.; Speck, J. S.; Schwartz, R. W.; Dimos, D.; Lockwood, S. J. *J. Mater. Res.* **1996**, *11*, 2076–2084.
(27) Shturman, I.; Shter, G. E.; Etin, A.; Grader, G. S. *Thin Solid Films* **2009**, *8*, 2767–2774.
(28) Yang, X.; Cheng, J.; Yu, S.; Chen, F.; Meng, Z. *J. Cryst. Growth* **2008**, *310*, 3466–3469.
(29) Dissado, L. A. *J. Phys. D* **1990**, *23*, 1582.
(30) Scott, J. F.; Melnick, B. M.; McMillan, L. D.; De Araujo, C. A. P. *Integr. Ferroelectr.* **1993**, *3*, 225–243.
(31) Yoshimura, M.; Bowen, H. K. *J. Am. Ceram. Soc.* **1981**, *7*, 404–410.
(32) O'Dwyer, J. J. *IEEE Trans. Electr. Insul.* **1982**, *6*, 484–487.
(33) Wang, Y.; Hao, X.; Xu, J. *J. Mater. Res.* **2012**, *27*, 1770–1775.
(34) Sigman, J.; Brennecka, G. L.; Clem, P. G.; Tuttle, B. A. *J. Am. Ceram. Soc.* **2008**, *91*, 1851–1857.
(35) Hao, X.; Yue, Z.; Xu, J.; An, S.; Nan, C. W. *J. Appl. Phys.* **2011**, *110*, 064109.
(36) von Schweidler, E. *Ann. Phys.* **1907**, *329*, 711–770.
(37) Cho, S. M.; Jeon, D. Y. *Thin Solid Films* **1999**, *1*, 149–154.
(38) Ma, B.; Kwon, D. K.; Narayanan, M.; Balachandran, U. *J. Phys. D* **2008**, *41*, 205003.

Downloaded by UNIV OF CINCINNATI on August 31, 2015 | http://pubs.acs.org
Publication Date (Web): February 18, 2013 | doi: 10.1021/am302985u